Accurate measurement of ^{15}N–^{13}C residual dipolar couplings in nucleic acids

Christopher P. Jaroniec[a], Jérôme Boisbouvier[b], Izabela Tworowska[c], Edward
P. Nikonowicz[c] & Ad Bax[a]

[a]*Laboratory of Chemical Physics, National Institute of Diabetes and Digestive and Kidney Diseases, National
Institutes of Health, Bethesda, MD 20892-0520, USA;* [b]*Laboratoire de RMN, Institut de Biologie Structu-
rale, Jean-Pierre Ebel, UMR 5075, CNRS-CEA-UJF, 41 rue Jules Horowitz, 38027 Grenoble, Cedex 1,
France;* [c]*Department of Biochemistry and Cell Biology, Rice University, P.O. Box 1892 Houston, TX 77251,
USA*

Abstract

New 3D HCN quantitative J (QJ) pulse schemes are presented for the precise and accurate measurement
of one-bond ^{15}N$_{1/9}$–^{13}C$_{1'}$, ^{15}N$_{1/9}$–^{13}C$_{6/8}$, and ^{15}N$_{1/9}$–^{13}C$_{2/4}$ residual dipolar couplings (RDCs) in weakly
aligned nucleic acids. The methods employ ^{1}H–^{13}C multiple quantum (MQ) coherence or TROSY-type
pulse sequences for optimal resolution and sensitivity. RDCs are obtained from the intensity ratio of H$_{1'}$–
C$_{1'}$–N$_{1/9}$ (MQ-HCN-QJ) or H$_{6/8}$–C$_{6/8}$–N$_{1/9}$ (TROSY-HCN-QJ) correlations in two interleaved 3D NMR
spectra, with dephasing intervals of zero (reference spectrum) and $\sim 1/(2J_{NC})$ (attenuated spectrum). The
different types of ^{15}N–^{13}C couplings can be obtained by using either the 3D MQ-HCN-QJ or TROSY-
HCN-QJ pulse scheme, with the appropriate setting of the duration of the constant-time ^{15}N evolution
period and the offset of two frequency-selective ^{13}C pulses. The methods are demonstrated for a uni-
formly ^{13}C, ^{15}N-enriched 24-nucleotide stem-loop RNA sequence, helix-35ψ, aligned in the magnetic field
using phage Pf1. For measurements of RDCs systematic errors are found to be negligible, and experi-
ments performed on a 1.5 mM helix-35ψ sample result in an estimated precision of ca. 0.07 Hz for $^{1}D_{NC}$,
indicating the utility of the measured RDCs in structure validation and refinement. Indeed, for a com-
plete set of ^{15}N$_{1/9}$–^{13}C$_{1'}$, ^{15}N$_{1/9}$–^{13}C$_{6/8}$, and ^{15}N$_{1/9}$–^{13}C$_{2/4}$ dipolar couplings obtained for the stem nu-
cleotides, the measured RDCs are in excellent agreement with those predicted for an NMR structure of
helix-35ψ, refined using independently measured observables, including ^{13}C–^{1}H, ^{13}C–^{13}C and ^{1}H–^{1}H
dipolar couplings.

Introduction

Traditionally, methods for NMR structure deter-
mination of biological macromolecules in solution
have relied on the measurement of ^{1}H–^{1}H NOEs
and ^{3}J coupling constants (Wüthrich, 1986). While
in globular proteins a large number of NOE
restraints between protons separated by many resi-
dues can be obtained with relative ease, in nucleic

acids and other extended molecules the number of
long-range contacts is typically low, and it even can
be zero. The effect of this paucity of long-range
NOE restraints can be alleviated by measuring
residual dipolar couplings (RDCs), which provide
precise information about the orientation of inter-
nuclear vectors relative to a common alignment
tensor frame in molecules weakly aligned in the
magnetic field (Tolman et al., 1995; Tjandra et al.,

1997; Prestegard et al., 2000; Vermeulen et al., 2000). In nucleic acids, measurement of RDC restraints has been greatly facilitated by the introduction of isotopic ^{13}C and ^{15}N enrichment procedures (Batey et al., 1992; Nikonowicz et al., 1992; Zimmer and Crothers, 1995; Louis et al., 1998; Masse et al., 1998) and methods for inducing a weak degree of molecular alignment (Tjandra and Bax, 1997; Clore et al., 1998; Hansen et al., 1998; Rückert and Otting, 2000; Tycko et al., 2000; Sass et al., 2000). Consequently, RDC measurements have enabled detailed structural studies to be performed for a wide range of oligonucleotides (Bayer et al., 1999; Tjandra et al., 2000; Sibille et al., 2001; Warren and Moore, 2001; Bondensgaard et al., 2002; MacDonald and Lu, 2002; Padrta et al., 2002; Barbic et al., 2003; Lukavsky et al., 2003; McCallum and Pardi, 2003; Wu et al., 2003; D'Souza et al., 2004; Stefl et al., 2004).

Recently, a number of new techniques have been introduced for the measurement of one-bond, two-bond and long-range, homo- and heteronuclear RDCs in nucleic acids, including ^{1}H–^{13}C, ^{1}H–^{15}N, ^{1}H–^{31}P, ^{1}H–^{1}H, ^{13}C–^{13}C and ^{15}N–^{13}C interactions (Hennig et al., 2001; Wu et al., 2001; Zidek et al., 2001; Yan et al., 2002; Boisbouvier et al., 2003; Miclet et al., 2003; Boisbouvier et al., 2004; O'Neil-Cabello et al., 2004). In this work we focus our attention on the measurement of one-bond ^{15}N–^{13}C interactions involving the glycosidic nitrogen, N_1 and N_9 for pyrimidine and purine bases, respectively. Since the magnitude of the dipolar coupling constant is $D \propto \gamma_i \gamma_j / r_{ij}^3$, where γ_i and γ_j are the gyromagnetic ratios of the coupled spins and r_{ij} represents the internuclear distance, $^{1}D_{NC}$ is inherently roughly an order of magnitude smaller than $^{1}D_{CH}$ and $^{1}D_{NH}$, with typical values of $|^{1}D_{NC}| \leq 3$ Hz for weakly aligned nucleic acids (Zidek et al., 2001). However, despite their small magnitude, $^{1}D_{NC}$ interactions can be useful for nucleic acid structure validation and refinement if measured with sufficiently high precision (i.e., with uncertainties that are at least an order of magnitude smaller than the potential range of these couplings) (Padrta et al., 2002). To date, several methods for the measurement of $^{1}D_{NC}$ in nucleic acids have been proposed (Zidek et al., 2001; Yan et al., 2002). These experiments have enabled measurements of $^{1}D_{N1/9-C1'}$ and $^{1}D_{N1/9-C6/8}$ coupling constants from peak displacements in the ^{13}C dimensions of either 2D ^{1}H–^{13}C

spin-state-selective (S^3E) (Sørensen et al., 1997) correlation spectra (Zidek et al., 2001) or 3D MQ-HCN correlation spectra (Yan et al., 2002). While frequency-based methods, in general, have a number of advantages, including the simplicity of spectral analysis and the ability to simultaneously provide multiple couplings using the E.COSY principle (Griesinger et al., 1985), they are often not completely 'problem-free,' particularly for the measurement of small coupling constants. Specifically, the precision and accuracy of the measured J and dipolar couplings depend on the resonance linewidths, and thus long evolution times are typically required in the dimension in which the coupling is measured. In addition, even relatively minor lineshape or phase distortions can have a significant impact on the accuracy of the measured couplings. Finally, in experiments where S^3E-type schemes are not employed the splitting of resonances into multiplet components leads to spectral crowding and possible peak overlap. Some of these problems can be alleviated by using techniques which employ the principle of quantitative J correlation (Bax et al., 1994), where couplings are measured from resonance intensities rather than from resonance frequencies. Recently, a number of such quantitative J correlation methods have been successfully applied to the measurements of small ^{15}N–^{13}C, ^{13}C–^{13}C, ^{1}H–^{13}C and ^{1}H–^{1}H dipolar couplings in weakly aligned proteins, yielding high precision and accuracy (Chou et al., 2000; Wu and Bax, 2002; Meier et al., 2003; Jaravine et al., 2004; Jaroniec et al., 2004).

In this work we describe quantitative J correlation techniques for the measurement of ^{15}N–^{13}C RDCs in weakly aligned nucleic acids. For optimal resolution and sensitivity, the experiments are of the 3D HCN type and employ ^{1}H–^{13}C multiple quantum (MQ) coherence (for ribose $H_{1'}$–$C_{1'}$–$N_{1/9}$ correlations) and TROSY-type pulse sequences (for base $H_{6/8}$–$C_{6/8}$–$N_{1/9}$ correlations) (Zidek et al., 2001). The ^{15}N–^{13}C couplings are derived from modulation of the peak intensities by the magnitude of $^{1}J_{NC}$, and the pulse schemes yield $^{1}D_{N1/9-C1'}$, $^{1}D_{N1/9-C6/8}$ or $^{1}D_{N1/9-C2/4}$ depending on which nuclei are selected by frequency adjustment of the shaped pulses. The methods are demonstrated for a uniformly ^{13}C, ^{15}N-enriched 24-nucleotide stem-loop RNA sequence, ribosomal helix-35ψ. A complete set of ^{15}N$_{1/9}$–^{13}C$_{1'}$, ^{15}N$_{1/9}$–^{13}C$_{6/8}$, and ^{15}N$_{1/9}$–^{13}C$_{2/4}$ RDCs determined for the stem

nucleotides, is found to be in excellent agreement (rmsd of 0.1 Hz) with preliminary structures derived from $^{13}C–^1H$, $^{13}C–^{13}C$ and $^1H–^1H$ couplings, indicating the utility of the $^{15}N–^{13}C$ dipolar coupling restraints in nucleic acid structure validation and refinement.

Experimental section

Two samples of a uniformly ^{13}C, ^{15}N-enriched 24-nucleotide RNA oligomer corresponding to helix-35 of *E. coli* 23S ribosomal RNA and containing pseudouridine (ψ) at position 746 were used in the experiments. The nucleotide sequence of helix-35ψ is: GGGCUAAUGψUGAAAAAU-UAGCCC. For simplicity the nucleotides are identified as G37–C60 in this paper (instead of G737–C760). Both samples were prepared in identical fashion in Shigemi microcells (300 μl), and each contained 1.5 mM helix-35ψ, 17 mM NaCl, 17 mM potassium phosphate, and 0.03 mM EDTA in 99% D_2O, at pH 6.8 (uncorrected meter reading). In addition, one of the samples contained 25 mg/ml filamentous phage Pf1 (Hansen et al., 1998) purchased from Asla Biotech Ltd. (Riga, Latvia, http://www.asla-biotech.com/asla-phage.htm), and extensively dialyzed against the same buffer. For the Pf1 aligned sample the ^2H lock solvent quadrupole splitting was 28.3 Hz.

All NMR data were collected at 25 °C on a Bruker DMX500 spectrometer, using a cryogenic triple-resonance probehead equipped with z-axis pulsed field gradients. Typical acquisition parameters (used for $^1J_{N1/9–C1'}$ measurements) are: 3D MQ HCN ($H_{1'}–C_{1'}–N_{1/9}$) quantitative J (MQ-HCN-QJ), two 3D spectra were recorded in an interleaved manner using the pulse scheme of Figure 2a. Each spectrum was acquired as a 76* × 18* × 324* data matrix with acquisition times of 48.8 ms (t_1, ^{15}N), 29.9 ms (t_2, ^{13}C), and 64.6 ms (t_3, ^1H), using two scans per FID, and a total measurement time of 9 h for the pair of interleaved spectra; 3D TROSY-HCN ($H_{6/8}–C_{6/8}–N_{1/9}$) quantitative J (TROSY-HCN-QJ), two 3D spectra were recorded in an interleaved manner using the pulse scheme of Figure 2b. Each spectrum was acquired as a 76* × 32* × 324* data matrix with acquisition times of 48.8 ms (t_1, ^{15}N), 31.0 ms (t_2, ^{13}C), and 64.6 ms (t_3, ^1H), using two scans per

FID, and a total measurement time of 16 h for the pair of interleaved spectra. For the $^1J_{N1/9–C6/8}$ and $^1J_{N1/9–C2/4}$ measurements ^{15}N evolution times ranging from 28 to 43 ms were used (see Figure 2 legend for details), and the number of increments in the ^{15}N dimension was adjusted accordingly.

All spectra were processed and analyzed using NMRPipe (Delaglio et al., 1995). A 90°-shifted sine-squared window function was used in the ^1H (F_3) dimension, and the indirect ^{15}N (F_1) and ^{13}C (F_2) dimensions were processed using sine window functions shifted by 81°. Prior to Fourier transformation the data sets were zero-filled at least three-fold in each dimension. As is customary for other quantitative J experiments (Chou et al., 2000; Jaroniec et al., 2004), the precise peak positions were obtained from the high signal-to-noise reference spectra, and the intensities in the reference and attenuated spectra at these exact locations were measured using the 3D Fourier interpolation feature in NMRPipe. Note that the use of linear prediction to increase the spectral resolution in ^{13}C or ^{15}N dimensions of the quantitative J spectra is not recommended as such procedures can decrease the accuracy of the measured intensity. While the RDCs extracted from test spectra processed with and without linear prediction were in reasonable agreement with one another, we found that the RDCs obtained from spectra processed without linear prediction were in best agreement with the structure of helix-35ψ.

Results and discussion

Description of pulse schemes

The methods described in this work for the measurement of one-bond $^{15}N_{1/9}–^{13}C_{1'}$, $^{15}N_{1/9}–^{13}C_{6/8}$, and $^{15}N_{1/9}–^{13}C_{2/4}$ dipolar couplings (Figure 1) are based on well-known triple-resonance pulse sequences optimized for applications to nucleic acids, combined with the principles of quantitative J correlation (Bax et al., 1994). Therefore, only a brief discussion of the new experiments is provided below. $H_{1'}–C_{1'}–N_{1/9}$ and $H_{6/8}–C_{6/8}–N_{1/9}$ chemical shift correlations are established using 3D HCN pulse schemes (Farmer II et al., 1993; Sklenar et al., 1993) of the 'out-and-back' variety (Figure 2). For optimal resolution and sensitivity the pulse schemes employ the sensitivity- and gradient-
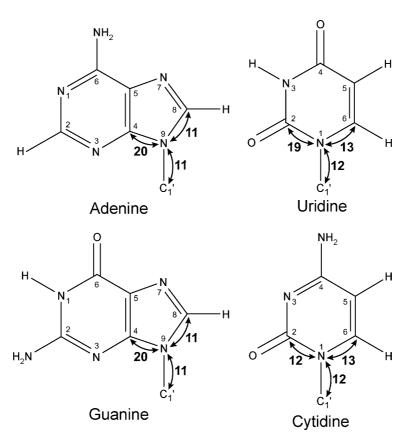
Figure 1. Dipolar couplings in nucleic acid bases measured in this work are marked with arrows. Approximate magnitudes of the relevant isotropic J coupling constants in Hz are indicated (Wijmenga and van Buuren, 1998).

enhanced pulse sequence elements (Kay et al., 1992; Brutscher et al., 1998; Pervushin et al., 1998b; Weigelt, 1998; Boisbouvier et al., 2000) and take advantage of the TROSY-effect, resulting from the interference between the $^{13}C_{6/8}$ chemical shift anisotropy and $^{13}C_{6/8}$–$^1H_{6/8}$ dipolar relaxation mechanisms (Brutscher et al., 1998; Pervushin et al., 1998a; Fiala et al., 2000) for the base ($H_{6/8}$–$C_{6/8}$–$N_{1/9}$) correlations, and of the favorable relaxation properties of $^1H_{1'}$–$^{13}C_{1'}$ MQ coherences (Griffey and Redfield, 1987; Grzesiek and Bax, 1995; Marino et al., 1997; Fiala et al., 2000) for the ribose ($H_{1'}$–$C_{1'}$–$N_{1/9}$) correlations.

Following $^1H \rightarrow {}^{13}C$ and $^{13}C \rightarrow {}^{15}N$ INEPT magnetization transfer steps and the 90° ^{15}N ϕ_1 pulse, the relevant part of the density matrix describing the transverse ^{15}N magnetization is given by $\rho = N_y C_z H_z$ for both pulse schemes. Note that during $^{13}C_{1'}$–^{15}N dephasing for the pulse scheme in Figure 2a, $^{13}C_{1'}$ evolves as $^{13}C_{1'}$–$^1H_{1'}$ MQ coherence, such as to minimize transverse

relaxation losses, while the frequency-selective nature of the 180° $H_{1'}$ pulse, centered at time $\tau + \delta$ after the initial 90° ^1H pulse, prevents dephasing by ^1H–^1H couplings (excepting the very small $^1H_{1'}$–$^1H_{1'}$ and $^1H_{1'}$–$^1H_5$ RDCs). A constant-time period of duration $2T$ is used to encode the ^{15}N chemical shift during t_1, with the concomitant modulation of the cross-peak intensity according to the magnitude of the $^{15}N_{1/9}$–$^{13}C_{1'}$, $^{15}N_{1/9}$–$^{13}C_{6/8}$, or $^{15}N_{1/9}$–$^{13}C_{2/4}$ coupling being active during the attenuated experiment and absent in the reference experiment (see below, and legend to Figure 2). Subsequently, magnetization is transferred back to $^1H_{1'}$ or $^1H_{6/8}$ for detection with a simultaneous encoding of the $^{13}C_{1'}$ or $^{13}C_{6/8}$ chemical shift, respectively, in t_2 during the constant-time (2δ) evolution period. For the $H_{1'}$–$C_{1'}$–$N_{1/9}$ experiments (Figure 2a), gradient encoding takes place during the short κ delays that precede the constant-time t_2 evolution period, which again takes place as $^{13}C_{1'}$–$^1H_{1'}$ MQ coherence, with a selective
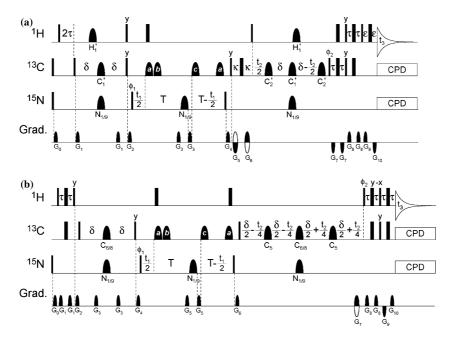
Figure 2. Pulse schemes of (A) 3D MQ-HCN-QJ ($H_{1'}–C_{1'}–N_{1/9}$) and (B) 3D TROSY-HCN-QJ ($H_{6/8}–C_{6/8}–N_{1/9}$) experiments. Narrow and wide rectangular pulses correspond to 90° and 180° flip angles, respectively. All pulses have phase x, unless indicated otherwise. Scheme (a), 3D MQ-HCN-QJ: The 180° $H_{1'}$ shaped pulses have the REBURP profile (Geen and Freeman, 1991), durations of 8 ms (at 500 MHz ^{1}H frequency), and are centered at 5.6 ppm. The 180° $N_{1/9}$ shaped pulses during the 2δ periods are of the IBURP-2 type, have durations of 2.0 ms (at 50.6 MHz ^{15}N frequency), and are centered at 157 ppm. The $N_{1/9}$ shaped pulse during the $2T$ period has the REBURP profile, duration of 1.5 ms, and is centered at 157 ppm. The 180° $C_{1'}$ shaped pulses during the 2δ periods have the REBURP profile, durations of 2.5 ms (at 125.6 MHz ^{13}C frequency), and are centered at 92.5 ppm. The 180° $C_{2'}$ shaped pulses during the second 2δ period (t_2) are of the IBURP-2 type, have durations of 2.5 ms, and are centered at 73.5 ppm. The ^{13}C shaped pulses applied during the $2T$ period are of the hyperbolic secant type (Silver et al., 1984) with squareness levels, μ, of 6. Pulses marked a have durations of 500 μs and are centered at 120 ppm. Pulses marked b and c, used to selectively reintroduce $J + D$ couplings between $N_{1/9}$ and $C_{1'}$, $C_{6/8}$ or $C_{2/4}$, have durations of 11 ms (corresponding to inversion bandwidths of $\pm$ 6 ppm) and are centered at 92.5 ppm (for measurement of $N_{1/9}–C_{1'}$ couplings), 140 ppm (for measurement of $N_{1/9}–C_{6/8}$ couplings) or 154 ppm (for measurement of $N_{1/9}–C_{2/4}$ couplings). The direction of the adiabatic sweep for pulse c is opposite to that used for pulse b; this compensates for minor systematic errors in measured J values due to spin evolution during the pulses. The position of the $H_{1'}$ shaped 180° pulse, applied during the t_2 constant-time evolution period, is fixed at the midpoint between the end of the second κ delay and the start of the $90_{\phi2}$ ^{13}C pulse. Reference and attenuated spectra are acquired in an interleaved manner. For the reference spectrum the ^{13}C pulses marked b and c are off (in practice applied at the minimum power level), and for the attenuated spectrum the pulses are applied as indicated in the figure. Delay durations: $\tau = 1.35$ ms, $\delta = 20$ ms, $\kappa = 0.65$ ms, $\epsilon = 0.35$ ms, $T = T' + t_a + t_b + t_G$, where t_a, t_b and t_G are the durations of ^{13}C shaped pulse a, ^{13}C shaped pulse b, and the gradient preceding the $N_{1/9}$ REBURP pulse. The delay T' is varied according to the type of ^{15}N–^{13}C coupling measured, and for optimal measurement sensitivity should be set to $\sim 1/(2J_{NC})$. In this work the following delays were used: $T = 25$ ms (for measurement $N_{1/9}–C_{1'}$ couplings), $T' = 21.5$ ms (for measurement of $N_{1/9}–C_{6/8}$ couplings), $T' = 14$ ms (for measurement of $N_{1/9}–C_{2/4}$ couplings for adenine, guanine and uridine) and $T' = 20$ ms (for measurement of $N_1–C_2$ couplings for cytidine). Phase cycling: $\phi_1 = x, -x$; $\phi_2 = -x$; receiver $= x, -x$. States-TPPI phase cycling of ϕ_1 is used to obtain quadrature detection in the ^{15}N (F_1) dimension. Quadrature in the ^{13}C (F_2) dimension is achieved using the gradient- and sensitivity-enhanced method in which two data sets are recorded for each t_2 increment: one set with the pulse phases indicated above, and a second set with phase $\phi_2 = x$ and the polarity of gradients G_5 and G_6 inverted. Pulsed field z-axis gradients are sine-bell shaped and have the following durations and strengths: $G_{0,1,2,3,4,5,6,7,8,9,10} = (1, 0.525, 0.73, 0.495, 0.62, 0.5, 0.5, 1.15, 1.15, 0.1415, 0.11$ ms) and (30, 30, 30, 30, 30, −30, 30, −10, 25, 30, −30 G/cm). Scheme (B), 3D TROSY-HCN-QJ: The majority of experimental parameters are identical to those described above for the 3D MQ-HCN-QJ scheme. Only the differences are highlighted. The 180° $C_{6/8}$ shaped pulses during the 2δ periods have the REBURP profile, duration of 2.5 ms, and are centered at 140 ppm. The 180° C_5 (cytidine and uridine) shaped pulses during the second 2δ period (t_2) are of the IBURP-2 type, have durations of 1.5 ms, and are centered at 100 ppm. Delay durations: $\tau = 1.25$ ms, $\delta = 15$ ms. Phase cycling: $\phi_1 = x, -x$; $\phi_2 = y$; receiver $= x, -x$. States-TPPI phase cycling of ϕ_1 is used to obtain quadrature detection in the ^{15}N (F_1) dimension. Quadrature in the ^{13}C (F_2) dimension is achieved using the gradient- and sensitivity-enhanced method in which two data sets are recorded for each t_2 increment: one set with the pulse phases indicated above, and a second set with phase $\phi_2 = -y$ and the polarity of gradient G_7 inverted. Pulsed field z-axis gradients are sine-bell shaped and have the following durations and strengths: $G_{0,1,2,3,4,5,6,7,8,9,10} = (3, 0.87, 0.615, 1.075, 0.525, 0.3, 0.665, 2, 0.95, 0.2515, 0.2515$ ms) and (6, 24, 24, 24, 24, 24, 24, 30, 24, −30, 30 G/cm).

180° $H_{1'}$ pulse preventing homonuclear ^1H–^1H dephasing.

In summary, two 3D $H_{1'}$–$C_{1'}$–$N_{1/9}$ (Figure 2a) or $H_{6/8}$–$C_{6/8}$–$N_{1/9}$ (Figure 2b) correlation spectra are recorded in an interleaved fashion such that either all ^{15}N–^{13}C couplings are decoupled (reference spectrum) or the ^{15}N antiphase coherences evolve under only one of the couplings (e.g., $^1J_{N1/9-C1'}$) (attenuated spectrum). Most ^{13}C spins in nucleic acids (in particular those with the largest couplings, i.e., $C_{1'}$, $C_{6/8}$, $C_{2/4}$, and purine C_5 nuclei) resonate in unique and relatively narrow regions of the ^{13}C spectrum (Wijmenga and van Buuren, 1998) and can be manipulated individually using frequency-selective pulses. Therefore, despite a relatively complex ^{15}N–^{13}C spin–spin coupling network in nucleotides (up to eight ^{13}C spins within three bonds of each $^{15}N_{1/9}$), measurement of the one-bond $^{15}N_{1/9}$–$^{13}C_{1'}$, $^{15}N_{1/9}$–$^{13}C_{6/8}$, and $^{15}N_{1/9}$–$^{13}C_{2/4}$ couplings is possible 'one-at-a-time', with minimal interference from multiple passive ^{15}N–^{13}C couplings. In order to maximize the dependence of the attenuated spectrum on the value of $^1J_{NC}$, the duration of the constant-time $^1J_{NC}$ dephasing period is adjusted to a 'null condition' with respect to the expected $^1J_{NC}$ value, i.e., 25–50 ms for typical $^1J_{NC}$ values in the 20–10 Hz range (Figure 1 and Supporting information). Considering the relatively uniform magnitude of $^1J_{NC}$ for each type of coupling (e.g., $N_{1/9}$–$C_{1'}$), irrespective of the nucleotide type (except cytidine $^1J_{N1-C2}$) (Figure 1), the RDCs within pyrimidine and purine bases can be obtained simultaneously and with near-optimal sensitivity from a single pair of interleaved 3D MQ-HCN-QJ and TROSY-HCN-QJ spectra. However, it is worth noting that for the four cytidine nucleotides in helix-35ψ, $^1D_{N1-C2}$ values obtained from independent measurements, optimized for either the measurement of adenine, guanine and uridine $^1D_{N1/9-C2/4}$ couplings or cytidine $^1D_{N1-C2}$ couplings, were in excellent agreement (rmsd < 0.1 Hz), despite the fact that one of the measurements was not optimized for cytidine $^1D_{N1-C2}$.

In practice the acquisition of reference and attenuated spectra is accomplished by turning *off* or *on*, respectively, the ^{13}C frequency-selective pulses (marked b and c in Figure 2) that are on-resonance with those ^{13}C spins for which $^1J_{NC}$ is to be measured. Shaped pulses marked a are broadband and of the hyperbolic secant type (Silver et al., 1984). When followed by frequency-selective

pulse b, all ^{13}C spins except for those excited by pulse b are inverted by the a/b pulse pair, and thereby decoupled. So, when pulses b and c are turned on, dephasing due to the selected $^1J_{NC}$ remains active. The value of $^1J_{NC}$ (or the sum, $^1J_{NC} + {}^1D_{NC}$, for the aligned sample) is obtained by fitting the experimental cross-peak intensity ratio in the reference and attenuated spectra to:

$$I_{att}/I_{ref} = \cos(2\pi {}^1J_{NC} T') \qquad (1)$$

where T' is slightly shorter than T, to account for the absence of net dephasing during the application of the ^{13}C decoupling pulses (see legend to Figure 2). RDCs, $^1D_{NC}$, are obtained as differences in the apparent $^1J_{NC}$ couplings measured in the isotropic and Pf1-aligned phases.

Application to helix-35ψ

Figure 3 shows representative strips, corresponding to the majority of the stem nucleotides, taken from the reference (A) and attenuated (B) 3D MQ-HCN-QJ ($H_{1'}$–$C_{1'}$–$N_{1/9}$) spectra adapted for the measurement of $^1J_{N1/9-C1'}$ recorded for $^{13}C/^{15}N$-enriched helix-35ψ, aligned in 25 mg/ml Pf1. Analogous spectra are obtained with the 3D MQ-HCN-QJ pulse scheme, adapted for the measurement of $^1J_{N1/9-C6/8}$ or $^1J_{N1/9-C2/4}$, and with the 3D TROSY-HCN-QJ ($H_{6/8}$–$C_{6/8}$–$N_{1/9}$) schemes. Overall, the measurements yield 66 $^{15}N_{1/9}$–$^{13}C_{1'}$, $^{15}N_{1/9}$–$^{13}C_{6/8}$, and $^{15}N_{1/9}$–$^{13}C_{2/4}$ dipolar couplings for 22 nucleotides of helix-35ψ (Table 1). No HCN correlations are obtained for pseudouridine, and correlations for A52 were too weak as a result of conformational exchange. The $^1D_{NC}$ values obtained using the MQ-HCN-QJ and TROSY-HCN-QJ methods are in excellent agreement. For example, a pairwise rms difference of ca. 0.1 Hz is obtained for independent measurements of the stem $N_{1/9}$–$C_{1'}$ and $N_{1/9}$–$C_{6/8}$ couplings (Figure 4). This is consistent with the uncertainties of 0.07 ± 0.03 Hz for the individual stem RDC measurements, estimated as described previously (see legend to Table 1) (Chou et al., 2000; Jaroniec et al., 2004), based on the average S/N ratios of ca. 160 ± 20 and 260 ± 40 in the reference spectra recorded for aligned and isotropic helix-35ψ samples, respectively. For the relatively strong alignment of the helix-35ψ sample used in the present study ($D_a^{CH} = -28.5$ Hz) $^1D_{NC}$ couplings potentially
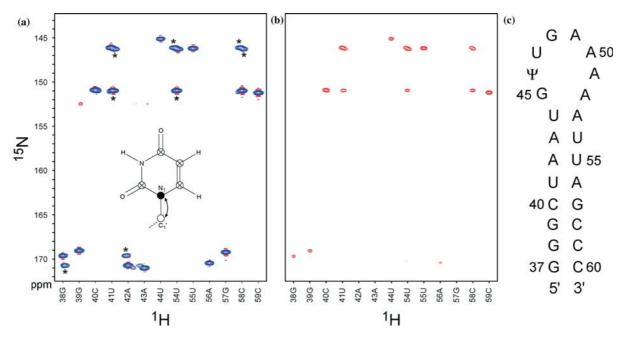
Figure 3. Cross sections taken from (a) reference and (b) attenuated 500 MHz 3D $H_{1'}-C_{1'}-N_{1/9}$ (MQ-HCN-QJ) correlation spectra adapted for the measurement of $^1J_{N1/9-C1'}$ recorded with $2T = 50$ ms, corresponding to the stem nucleotides of $^{13}C,^{15}N$-labeled helix-35ψ aligned in the magnetic field using 25 mg/ml Pf1. ^1H and ^{13}C frequencies are marked according to the nucleotide number, and positive and negative intensities are in blue and red, respectively. Cross-peaks arising from nucleotides from neighboring ^{13}C planes are denoted by asterisks. A typical nucleotide base is shown in the inset. The representative 3D MQ-HCN-QJ ($^1J_{N1/9-C1'}$) spectra shown in the figure report on the couplings ($\leftrightarrow$) between $^{15}N_{1/9}$ ($\bullet$) and $^{13}C_{1'}$ nuclei ($\bigcirc$), while the couplings between $^{15}N_{1/9}$ and all other ^{13}C spins ($\otimes$) are decoupled. $^1J_{N1/9-C6/8}$ and $^1J_{N1/9-C2/4}$ are obtained from analogous spectra (see text). (C) Primary structure of helix-35ψ.

could cover a range from −2.1 to +3 Hz, and compared to this range the measurement error is smaller by nearly two orders of magnitude. This indicates these $^1D_{NC}$ values are meaningful restraints during structure calculation. Interestingly, the observed $^1D_{NC}$ couplings cover only a relatively narrow range of ca. −2 to 0 Hz, indicating that all bases are oriented roughly orthogonal to the *z*-axis of the alignment tensor, which is approximately parallel to the helical axis of the A-form stem region. Remarkably, this applies not only to the stem nucleotides, but also to the loop.

Figure 5a shows the correlation between the measured $^1D_{NC}$ values and those calculated for the stem region of the helix-35ψ structure. We compare the full set of 42 $^{15}N_{1/9}-^{13}C_{1'}$, $^{15}N_{1/9}-^{13}C_{6/8}$, and $^{15}N_{1/9}-^{13}C_{2/4}$ dipolar couplings obtained for the stem nucleotides (G38-U44 and A53-C59) with those predicted for an NMR structure of helix-35ψ (unpublished results), derived from $^{13}C-^1H$, $^{13}C-^{13}C$ and $^1H-^1H$ RDCs (Miclet et al., 2003; Boisbouvier et al., 2004; O'Neil-Cabello et al., 2004). Excellent agreement

between measured and predicted couplings is obtained when performing a singular value decomposition (SVD) fit (Losonczi et al., 1999; Sass et al., 1999) of the 42 stem RDCs to the NMR structure. A Pearson's correlation coefficient, R_P, of 0.97 is obtained when comparing measured and predicted couplings, corresponding to a quality factor, *Q*, of 0.08. The rms difference between measured and predicted couplings of 0.10 Hz is only slightly larger than the 0.07 Hz precision of the measurement. Interestingly, a significantly poorer fit is obtained when best-fitting the RDCs to a model A-form RNA helix, generated using the program InsightII (Figure 5b). The nearly three-fold increase, observed in the quality factor and rmsd between the measured and predicted $^{15}N-^{13}C$ couplings for the idealized A-form helix vs. the refined helix-35ψ structure, indicates that high precision measurements of base $^{13}C-^1H$, $^{13}C-^{13}C$, and $^{15}N-^{13}C$ RDCs can be used to report on slight deviations from "ideal" base pair geometry in nucleic acids.

Table 1. One-bond ^{15}N–^{13}C residual dipolar couplings measured for helix-35ψ

Nucleotide	$^1D_{\mathrm{N1/9-C1'}}$ (Hz)	$^1D_{\mathrm{N1/9-C6/8}}$ (Hz)	$^1D_{\mathrm{N1/9-C2/4}}$ (Hz)
G37	−1.14 ± 0.35	−0.76 ± 0.43	−0.74 ± 0.56
G38	−1.25 ± 0.07	−1.36 ± 0.08	−0.38 ± 0.11
G39	−1.46 ± 0.05	−0.77 ± 0.06	−0.95 ± 0.08
C40	−1.25 ± 0.03	−0.57 ± 0.04	−1.34 ± 0.05
U41	−0.84 ± 0.04	−0.79 ± 0.05	−1.97 ± 0.08
A42	−0.81 ± 0.06	−1.33 ± 0.08	−1.89 ± 0.09
A43	−0.87 ± 0.06	−1.77 ± 0.07	−1.30 ± 0.11
U44	−1.30 ± 0.08	−1.86 ± 0.09	−1.09 ± 0.14
G45	−1.33 ± 0.20	−1.12 ± 0.20	−1.33 ± 0.30
U47	−0.23 ± 0.04	−0.83 ± 0.04	−0.48 ± 0.07
G48	0.05 ± 0.04	−0.86 ± 0.04	−0.20 ± 0.07
A49	−0.63 ± 0.03	−0.59 ± 0.03	−0.47 ± 0.06
A50	−0.62 ± 0.03	−0.44 ± 0.04	−0.68 ± 0.08
A51	−0.29 ± 0.25	0.03 ± 0.30	−1.29 ± 0.43
A53	−1.16 ± 0.08	−1.42 ± 0.09	−0.80 ± 0.16
U54	−1.32 ± 0.06	−1.04 ± 0.06	−1.25 ± 0.12
U55	−1.38 ± 0.05	−1.04 ± 0.06	−1.65 ± 0.09
A56	−1.06 ± 0.09	−1.17 ± 0.11	−2.04 ± 0.13
G57	−0.78 ± 0.06	−1.44 ± 0.06	−1.49 ± 0.08
C58	−0.74 ± 0.03	−2.12 ± 0.04	−0.90 ± 0.05
C59	−1.23 ± 0.03	−1.68 ± 0.04	−0.34 ± 0.06
C60	−1.12 ± 0.03	−1.01 ± 0.03	−0.15 ± 0.05

Uncertainties for the individual $^1D_{\mathrm{NC}}$ values were calculated as $\Delta D = (\Delta J^2_{\mathrm{isotropic}} + \Delta J^2_{\mathrm{aligned}})^{1/2}$ with $\Delta J = 1/(2\pi\,\theta\,T\,')$, where θ is the signal-to-noise ratio in the reference spectrum (Chou et al., 2000; Jaroniec et al., 2004). In cases where more than one measurement of the same $^1D_{\mathrm{NC}}$ was available, the average of the measurements is reported, with the exception of loop U47–A50 couplings where values obtained from 3D TROSY-HCN-QJ experiments are given. Conformational exchange leads to a decreased signal-to-noise ratio for loop ribose $H_{1'}$–$C_{1'}$–$N_{1/9}$ correlations in MQ-HCN-QJ spectra (with three-fold lower S/N on-average relative to stem nucleotides), resulting in an average uncertainty of ±0.27 Hz for $^1D_{\mathrm{NC}}$ for these measurements. Note that the reported dipolar couplings take into account the negative signs of γ_N and the isotropic $^1J_{\mathrm{NC}}$ couplings (see Supporting information).

Sources of measurement error

During data analysis we have considered several sources of systematic error, which could possibly adversely affect the accuracy of the $^1D_{\mathrm{NC}}$ measurements. These include (i) passive ^{15}N–^{13}C couplings, (ii) incomplete ^{13}C isotopic enrichment and (iii) pulse imperfections. These types of errors have been discussed in detail previously in the context of quantitative J methods applied to weakly aligned proteins (Chou et al., 2000; Jaroniec et al.,
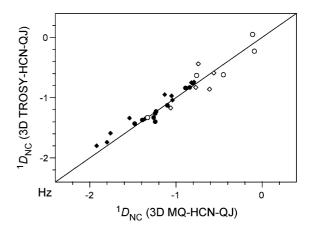

Figure 4. Comparison of $^1D_{\mathrm{NC}}$ values measured from 3D MQ-HCN-QJ ($H_{1'}$–$C_{1'}$–$N_{1/9}$) and TROSY-HCN-QJ ($H_{6/8}$–$C_{6/8}$–$N_{1/9}$) spectra. The measurements are plotted separately for $N_{1/9}$–$C_{1'}$ and $N_{1/9}$–$C_{6/8}$ couplings, and for stem and loop nucleotides as follows: stem $N_{1/9}$–$C_{1'}$ (●), loop $N_{1/9}$–$C_{1'}$ (○), stem $N_{1/9}$–$C_{6/8}$ (◆), loop $N_{1/9}$–$C_{6/8}$ (◇). The correlation coefficient for all $^1D_{\mathrm{NC}}$ measurements is 0.96, and the pairwise rms differences according to the coupling type are: 0.06 Hz for stem $N_{1/9}$–$C_{1'}$; 0.13 Hz for loop $N_{1/9}$–$C_{1'}$; 0.12 Hz for stem $N_{1/9}$–$C_{6/8}$; and 0.18 Hz for loop $N_{1/9}$–$C_{6/8}$. The negative sign of all observed $^1D_{\mathrm{NC}}$ RDCs includes the negative sign of γ_N, i.e., larger J_{CN} splittings were observed in the aligned state than in the isotropic phase.

2004). As discussed briefly below, they turn out to be mostly negligible for weakly aligned nucleic acids.

Only those passive couplings which are decoupled in the reference spectrum but contribute to the dephasing of transverse coherences in the attenuated spectrum lead to systematic errors in the measured RDCs (Chou et al., 2000; Jaroniec et al., 2004). Consequently, due to the unique resonance frequencies of the relevant ^{13}C nuclei, the measurements of $N_{1/9}$–$C_{1'}$, $N_{1/9}$–$C_{6/8}$ and pyrimidine N_1–C_2 couplings are essentially free of systematic errors due to passive couplings. However, for purine bases, where the C_4 and C_2 spins have nearly identical resonance frequencies, the $^3J_{\mathrm{N9-C2}}$ coupling of ∼3–4 Hz (Wijmenga and van Buuren, 1998) must at least be considered in the measurement of $^1J_{\mathrm{N9-C4}}$. Simulations indicate that for longer dephasing times, the presence of the passive $^3J_{\mathrm{N9-C2}}$ coupling can lead to significant systematic errors in the measurement of $^1J_{\mathrm{N9-C4}}$ and $^1D_{\mathrm{N9-C4}}$ when using the single-coupling model of Equation 1. The systematic error scales with the size of the difference between $^1J_{\mathrm{N9-C4}} + {}^1D_{\mathrm{N9-C4}}$ and the $^1J_{\mathrm{N9-C4}}$ target value used for calculating the dephasing time. For the present study, where

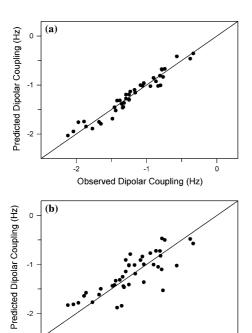*Figure 5.* (a) Correlation between $^1D_{NC}$ values obtained from 3D MQ-HCN-QJ and TROSY-HCN-QJ spectra and values predicted for helix-35ψ. The alignment tensor was derived from the best-fit of the measured dipolar couplings to a typical low-energy NMR structure of helix-35ψ refined using independently measured observables, including ^{13}C–^1H, ^{13}C–^{13}C and ^1H–^1H RDCs. Nearly identical fits are obtained for other low-energy structures from the ensemble. A total of 42 $N_{1/9}$–$C_{1'}$, $N_{1/9}$–$C_{6/8}$ and $N_{1/9}$–$C_{2/4}$ couplings obtained for the stem nucleotides (G38-U44 and A53-C59) of helix-35ψ are included in the fit. The correlation coefficient, R_P, equals 0.97, and the quality factor, Q, equals 0.08, with an rmsd between measured and predicted dipolar couplings of 0.10 Hz. (b) Correlation between the 42 stem $^1D_{NC}$ values and those predicted for an idealized RNA A-form helix, generated for the terminal eight base pairs using the Biopolymer module in Insight II (Molecular Simulations, Inc.). The fit parameters are $R_P = 0.78$, $Q = 0.21$, and rmsd $= 0.26$ Hz.

$2T \approx 1/(2 \times {}^1J_{N9-C4})$, the resulting systematic error in $^1D_{N9-C4}$ is at most ca. 0.1 Hz for dipolar couplings as large as ± 2 Hz.

While incomplete ^{13}C labeling leads to systematic errors in the measurement of $^1J_{NC}$ for most experiments (except $H_{1'}$–$C_{1'}$–$N_{1/9}$ MQ-HCN-QJ correlation spectra adapted for the measurement of $^1J_{N1/9-C1'}$ and $H_{6/8}$–$C_{6/8}$–$N_{1/9}$ TROSY-HCN-QJ correlation spectra adapted for the measurement of $^1J_{N1/9-C6/8}$, where only magnetization corresponding to $^{15}N_{1/9}$–$^{13}C_{1'}$ and $^{15}N_{1/9}$–$^{13}C_{6/8}$ spin-pairs, respectively, is detected), the

measurements of corresponding $^1D_{NC}$ are largely unaffected as discussed in detail previously (Jaroniec et al., 2004). This is supported by simulations of systematic errors resulting from incomplete ^{13}C labeling (see Supporting information), which indicate that for ^{13}C labeling efficiencies of 90% or higher, errors of at most ca. 0.2 Hz are introduced for dipolar couplings as large as ± 2 Hz. Experimental validation can be found in the absence of a systematic difference in Figure 4, which compares $^1D_{N1/9-C1'}$ and $^1D_{N1/9-C6/8}$ values resulting from schemes that are intrinsically sensitive to incomplete labeling with those that are not. For stem nucleotides the rms difference between $^1D_{NC}$ obtained using the different methods is ca. 0.1 Hz, consistent with the uncertainties of the individual measurements due to random noise. The approximately two-fold increase in the rms difference in $^1D_{NC}$ for loop nucleotides correlates well with the two- to four-fold decrease in the signal-to-noise ratio for loop ribose $H_{1'}$–$C_{1'}$–$N_{1/9}$ correlations in MQ-HCN-QJ spectra relative to the stem correlations.

Finally, we have considered the effects of spin evolution during the long hyperbolic secant ^{13}C pulses on the accurate measurement of $^1J_{NC}$. Although these pulses have a symmetric excitation profile, simulations and experiments (data not shown) indicate that for off-resonance ^{13}C spins within the excitation bandwidth of the hyperbolic secant pulses, the anti-phase ^{15}N coherences evolve under $^1J_{NC}$ for a time proportional to the offset of a given ^{13}C from the carrier center-frequency. While this relatively minor effect is not expected to significantly affect the accurate measurement of $^1D_{NC}$, it is completely eliminated for a pair of hyperbolic secant pulses by setting the direction of the adiabatic sweep for the second pulse (pulse c in Figure 2) to be opposite to that for the first pulse (pulse b).

Concluding remarks

The new 3D HCN quantitative J methods described in this work yield spectra with high resolution and sensitivity, and afford precise and accurate measurements of $^{15}N_{1/9}$–$^{13}C_{1'}$, $^{15}N_{1/9}$–$^{13}C_{6/8}$, and $^{15}N_{1/9}$–$^{13}C_{2/4}$ RDCs in weakly aligned nucleic acids. $^1D_{NC}$ involving the glycosidic $N_{1/9}$ can be obtained using either the 3D MQ-HCN-QJ ($H_{1'}$–C_1–$N_{1/9}$) or

TROSY-HCN-QJ ($H_{6/8}$–$C_{6/8}$–$N_{1/9}$) methods with minimal adjustment of the pulse scheme parameters. Minimum duration (two scans per FID) overnight experiments carried out on a 1.5 mM 24-nt RNA sample using a cryogenic probehead at 500 MHz, result in an uncertainty of ca. 0.07 Hz for $^1D_{NC}$. For a complete set of 42 $^{15}N_{1/9}$–$^{13}C_{1'}$, $^{15}N_{1/9}$–$^{13}C_{6/8}$, and $^{15}N_{1/9}$–$^{13}C_{2/4}$ dipolar couplings obtained for 14 stem nucleotides, the measured RDCs are in excellent agreement with those predicted for an NMR structure derived from independently measured ^{13}C–^1H, ^{13}C–^{13}C and ^1H–^1H RDCs. These observations validate the new experiments and confirm the utility of ^{15}N–^{13}C RDCs for nucleic acid structure calculation and refinement. The new pulse schemes are straightforward to implement, and we have shown that a simple, single-parameter model can be used to extract accurate values of $^1D_{NC}$.

Although we have demonstrated the quantitative J methods for a 24-nt RNA with a rotational correlation time of ca. 5.4 ns at 25°C (J. Boisbouvier, unpublished data), we expect the methods to also be applicable to larger systems. Signal-to-noise ratios of 20:1–30:1 in reference spectra are required to obtain uncertainties of ± 0.5 Hz in ^{15}N–^{13}C RDCs. Although such errors generally will be too large to refine base-pair geometry in an A-form helix, they often will be acceptable when, for example, determining the relative orientation of two helical fragments. In order to evaluate experimentally the performance of the experiments for slower tumbling systems, we recorded HCN reference spectra using a ^{15}N constant-time period of $2T' = 50$ ms (maximum duration used in the QJ experiments) on helix-35ψ at 500 MHz ^1H frequency and 8 °C, where the effective rotational correlation time of helix-35ψ due to the lower temperature and higher viscosity of D_2O (Cho et al., 1999) is ca. 9.5 ns. This resulted, on average, in a S/N decrease by a factor of 3.5–4 relative to 25 °C. This indicates that under those conditions, a minimum duration (two scans per FID) overnight 3D MQ-HCN-QJ or TROSY-HCN-QJ experiment carried out using a cryogenic probehead on a 1.5 mM RNA sample at 500 MHz, will yield an average S/N ratio of ca. 40:1–50:1, corresponding to a random error in $^1D_{CN}$ of ca. 0.25 Hz. The relatively favorable behavior of the experiment for slower tumbling systems is due in part to the long transverse relaxation time of the $^{15}N_{1/9}$ spins, which we measured to be ca. 125 ms for helix-35ψ at 500 MHz, 25 °C. The favorable spin-spin relaxation rates for $^1H_{1'}$–$^{13}C_{1'}$ MQ coherence and the TROSY $^{13}C_{6/8}$–$^1H_{6/8}$ doublet component (Zidek et al., 2001) are also important to the applicability of the experiments to slower tumbling systems.

Supporting information available

One table containing the one-bond ^{15}N–^{13}C isotropic J couplings measured for helix-35ψ, and one figure demonstrating the effect of incomplete ^{13}C enrichment on the measurement of $^1J_{NC}$. This table and figure are available in electronic form at: http://dx.doi.org/10.1007/s10858-005-0646-2. Pulse sequence code for Bruker Avance spectrometers can be found at http://spin.niddk.nih.gov/bax/.

Acknowledgements

References

Barbic, A., Zimmer, D.P. and Crothers, D.M. (2003) *Proc. Natl. Acad. Sci. USA*, **100**, 2369–2373.

Batey, R.T., Inada, M., Kujawinski, E., Puglisi, J.D. and Williamson, J.R. (1992) *Nucleic Acid Res.*, **20**, 4515–4523.

Bax, A., Vuister, G.W., Grzesiek, S., Delaglio, F., Wang, A.C., Tschudin, R. and Zhu, G. (1994) *Meth. Enzymol.*, **239**, 79–105.

Bayer, P., Varani, L. and Varani, G. (1999) *J. Biomol. NMR*, **14**, 149–155.

Boisbouvier, J., Brutscher, B., Pardi, A., Marion, D. and Simorre, J.P. (2000) *J. Am. Chem. Soc.*, **122**, 6779–6780.

Boisbouvier, J., Bryce, D.L., O'Neil-Cabello, E., Nikonowicz, E.P. and Bax, A. (2004) *J. Biomol. NMR*, **30**, 287–301.

Boisbouvier, J., Delaglio, F. and Bax, A. (2003) *Proc. Natl. Acad. Sci. USA*, **100**, 11333–11338.

Bondensgaard, K., Mollova, E.T. and Pardi, A. (2002) *Biochemistry*, **41**, 11532–11542.

Brutscher, B., Boisbouvier, J., Pardi, A., Marion, D. and Simorre, J.-P. (1998) *J. Am. Chem. Soc.*, **120**, 11845–11851.

Cho, C.H., Urquidi, J., Singh, S. and Robinson, G.W. (1999) *J. Phys. Chem. B*, **103**, 1991–1994.

Chou, J.J., Delaglio, F. and Bax, A. (2000) *J. Biomol. NMR*, **18**, 101–105.

Clore, G.M., Starich, M.R. and Gronenborn, A.M. (1998) *J. Am. Chem. Soc.*, **120**, 10571–10572.

Delaglio, F., Grzesiek, S., Vuister, G.W., Zhu, G., Pfeifer, J. and Bax, A. (1995) *J. Biomol. NMR*, **6**, 277–293.

D'Souza, V., Dey, A., Habib, D. and Summers, M.F. (2004) *J. Mol. Biol.*, **337**, 427–442.

Farmer, B.T. II, Mueller, L., Nikonowicz, E.P. and Pardi, A. (1993) *J. Am. Chem. Soc.*, **115**, 11040–11041.

Fiala, R., Czernek, J. and Sklenar, V. (2000) *J. Biomol. NMR*, **16**, 291–302.

Geen, H. and Freeman, R. (1991) *J. Magn. Reson.*, **93**, 93–141.

Griesinger, C., Sørensen, O.W. and Ernst, R.R. (1985) *J. Am. Chem. Soc.*, **107**, 6394–6396.

Griffey, R.H. and Redfield, A.G. (1987) *Q. Rev. Biophys.*, **19**, 51–82.

Grzesiek, S. and Bax, A. (1995) *J. Biomol. NMR*, **6**, 335–339.

Hansen, M.R., Mueller, L. and Pardi, A. (1998) *Nat. Struct. Biol.*, **5**, 1065–1074.

Hennig, M., Carlomagno, T. and Williamson, J.R. (2001) *J. Am. Chem. Soc.*, **123**, 3395–3396.

Jaravine, V.A., Cordier, F. and Grzesiek, S. (2004) *J. Biomol. NMR*, **29**, 309–318.

Jaroniec, C.P., Ulmer, T.S. and Bax, A. (2004) *J. Biomol. NMR*, **30**, 181–194.

Kay, L.E., Keifer, P. and Saarinen, T. (1992) *J. Am. Chem. Soc.*, **114**, 10663–10665.

Losonczi, J.A., Andrec, M., Fischer, M.W.F. and Prestegard, J.H. (1999) *J. Magn. Reson.*, **138**, 334–342.

Louis, J.M., Martin, R.G., Clore, G.M. and Gronenborn, A.M. (1998) *J. Biol. Chem.*, **273**, 2374–2378.

Lukavsky, P.J., Kim, I., Otto, G.A. and Puglisi, J.D. (2003) *Nat. Struct. Biol.*, **10**, 1033–1038.

MacDonald, D. and Lu, P. (2002) *Curr. Opin. Struct. Biol.*, **12**, 337–343.

Marino, J.P., Diener, J.L., Moore, P.B. and Griesinger, C. (1997) *J. Am. Chem. Soc.*, **119**, 7361–7366.

Masse, J.E., Bortmann, P., Dieckmann, T. and Feigon, J. (1998) *Nucleic Acid Res.*, **26**, 2618–2624.

McCallum, S.A. and Pardi, A. (2003) *J. Mol. Biol.*, **326**, 1037–1050.

Meier, S., Haussinger, D., Jensen, P., Rogowski, M. and Grzesiek, S. (2003) *J. Am. Chem. Soc.*, **125**, 44–45.

Miclet, E., O'Neil-Cabello, E., Nikonowicz, E.P. and Bax, A. (2003) *J. Am. Chem. Soc.*, **125**, 15740–15741.

Nikonowicz, E.P., Sirr, A., Legault, P., Jucker, F.M., Baer, L.M. and Pardi, A. (1992) *Nucleic Acid Res.*, **20**, 4507–4513.

O'Neil-Cabello, E., Bryce, D.L., Nikonowicz, E.P. and Bax, A. (2004) *J. Am. Chem. Soc.*, **126**, 66–67.

Padrta, P., Stefl, R., Kralik, L., Zidek, L. and Sklenar, V. (2002) *J. Biomol. NMR*, **24**, 1–14.

Pervushin, K., Riek, R., Wider, G. and Wuthrich, K. (1998a) *J. Am. Chem. Soc.*, **120**, 6394–6400.

Pervushin, K., Wider, G. and Wuthrich, K. (1998b) *J. Biomol. NMR*, **12**, 345–348.

Prestegard, J.H., Al-Hashimi, H.M. and Tolman, J.R. (2000) *Q. Rev. Biophys.*, **33**, 371–424.

Rückert, M. and Otting, G. (2000) *J. Am. Chem. Soc.*, **122**, 7793–7797.

Sass, J., Cordier, F., Hoffmann, A., Rogowski, M., Cousin, A., Omichinski, J.G., Lowen, H. and Grzesiek, S. (1999) *J. Am. Chem. Soc.*, **121**, 2047–2055.

Sass, H.J., Musco, G., Stahl, S.J., Wingfield, P.T. and Grzesiek, S. (2000) *J. Biomol. NMR*, **18**, 303–309.

Sibille, N., Pardi, A., Simorre, J.P. and Blackledge, M. (2001) *J. Am. Chem. Soc.*, **123**, 12135–12146.

Silver, M.S., Joseph, R.I. and Hoult, D.I. (1984) *J. Magn. Reson.*, **59**, 347–351.

Sklenar, V., Peterson, R.D., Rejante, M.R. and Feigon, J. (1993) *J. Biomol. NMR*, **3**, 721–727.

Sørensen, M.D., Meissner, A. and Sørensen, O.W. (1997) *J. Biomol. NMR*, **10**, 181–186.

Stefl, R., Wu, H.H., Ravindranathan, S., Sklenar, V. and Feigon, J. (2004) *Proc. Natl. Acad. Sci. USA*, **101**, 1177–1182.

Tjandra, N. and Bax, A. (1997) *Science*, **278**, 1111–1114.

Tjandra, N., Omichinski, J.G., Gronenborn, A.M., Clore, G.M. and Bax, A. (1997) *Nat. Struct. Biol.*, **4**, 732–738.

Tjandra, N., Tate, S., Ono, A., Kainosho, M. and Bax, A. (2000) *J. Am. Chem. Soc.*, **122**, 6190–6200.

Tolman, J.R., Flanagan, J.M., Kennedy, M.A. and Prestegard, J.H. (1995) *Proc. Natl. Acad. Sci. USA*, **92**, 9279–9283.

Tycko, R., Blanco, F.J. and Ishii, Y. (2000) *J. Am. Chem. Soc.*, **122**, 9340–9341.

Vermeulen, A., Zhou, H.J. and Pardi, A. (2000) *J. Am. Chem. Soc.*, **122**, 9638–9647.

Warren, J.J. and Moore, P.B. (2001) *J. Biomol. NMR*, **20**, 311–323.

Weigelt, J. (1998) *J. Am. Chem. Soc.*, **120**, 10778–10779.

Wijmenga, S.S. and Buuren, B.N.M.van (1998) *Prog. Nucl. Magn. Reson. Spectrosc.*, **32**, 287–387.

Wu, Z.R. and Bax, A. (2002) *J. Am. Chem. Soc.*, **124**, 9672–9673.

Wu, Z.G., Delaglio, F., Tjandra, N., Zhurkin, V.B. and Bax, A. (2003) *J. Biomol. NMR*, **26**, 297–315.

Wu, Z.R., Tjandra, N. and Bax, A. (2001) *J. Biomol. NMR*, **19**, 367–370.

Wüthrich, K. (1986) *NMR of Proteins and Nucleic Acids*, Wiley, New York, NY.

Yan, J.L., Corpora, T., Pradhan, P. and Bushweller, J.H. (2002) *J. Biomol. NMR*, **22**, 9–20.

Zidek, L., Wu, H., Feigon, J. and Sklenar, V. (2001) *J. Biomol. NMR*, **21**, 153–160.

Zimmer, D.P. and Crothers, D.M. (1995) *Proc. Natl. Acad. Sci. USA*, **92**, 3091–3095.